UNIVERSITY OF CALIFORNIA, SAN DIEGO

# Stretchable Graphene Barriers for Organic Optoelectronic Devices

A Thesis submitted in partial satisfaction of the requirements for the degree Master of Science

in

Nanoengineering

by

Casey Kong

Committee in Charge:

Professor Darren Lipomi, Chair
Professor Prabhakar Bandaru
Professor Donald Sirbuly

2015

The Thesis of Casey Kong is approved, and it is acceptable in quality and form for publication on microfilm and electronically:

_____

_____

_____

Chair

University of California, San Diego

2015

TABLE OF CONTENTS

LIST OF FIGURES

ABSTRACT OF THE THESIS

Stretchable Graphene Barriers for Organic Optoelectronic Devices

by

Casey Kong

Master of Science in Nanoengineering

University of California, San Diego, 2015

Professor Darren Lipomi, Chair

This thesis describes the use of a transparent, stretchable gas barrier film used to encapsulate organic devices in order to protect them from chemical degradation. One of the major issues with current organic semiconductor materials is that they are susceptible to degradation when exposed to oxygen and water vapor in the ambient atmosphere. In order to take advantage of these materials, stretchable barrier films must also be developed.

Solar cell devices were fabricated using an organic bulk heterojunction blend of poly(3-heptylthiophene) and phenyl-$C_{61}$-butyric acid methyl ester (P3HpT:PCBM).

Stretchable barrier films were fabricated with graphene and polyurethane (PU) using a simple dip coating process. Devices encapsulated with an unstrained graphene/PU barrier film retained 60.6 ± 3.7% efficiency after 10 days, exhibiting barrier properties similar to that of a control device encapsulated with glass (61.1 ± 3.2%). Measurements over the course of 1 day showed that graphene/PU films strained up to 20% were still able to maintain 91.5 ± 2.8% efficiency. Electrical resistance measurements showed that graphene cracks around 6% strain. This work highlights the potential impact graphene/PU barrier films may have on stretchable electronics.

## Introduction

There are many ways in which the materials used in organic electronics degrade. One of the major degradation mechanisms of organic electronics is degradation through exposure to oxygen and water vapor in the ambient atmosphere.[1–3] Intrinsically stretchable electronics have a broad range of applications in the field of bio-medical electronic skins,[4] photovoltaic devices,[5] soft robotics,[6] and wearable technology.[7] Currently, the majority of fabricated organic devices are kept in a glove box under a nitrogen atmosphere to prevent degradation. However, if these organic devices are to be used in any large-scale application, effective barrier materials to prevent degradation must be developed. Recently, organic solar cells have reached a record efficiency of 10%.[8,9]

Graphene is a 2D lattice of $sp^2$-hybridized carbon atoms that has been shown to be theoretically impermeable to all liquids and gases.[10] Graphene has promising applications in the field of stretchable electronics due to its inherent strength, thinness, and barrier properties.[11] By transferring graphene onto a polyurethane substrate, we have developed a stretchable, transparent barrier film that can be used to extend the lifetime of organic electronics in ambient atmosphere. In order to characterize the effectiveness of these barrier films, we encapsulated organic solar cell devices using these barriers and measured the rate of degradation in the devices. Furthermore, we measured the intrinsic stretchability of these film through scanning electron microscopy and electrical resistance measurements.

# Chapter 1

## 1.1 Background

The degradation of organic semiconducting polymers in ambient atmosphere has been a well-documented issue. There are two main routes in solving the issue of degradation in organic materials. The first solution would be to circumvent the intrinsic susceptibility of these organic materials to degradation in ambient atmosphere by developing new materials that are stable in air.[12] The second solution would be to develop barrier materials that can achieve extremely low water vapor and oxygen transmission rates. Currently, there are a variety of effective barrier materials ranging in complexity from simple glass to thin films fabricated using layer by layer deposition.[13–15] The issue with many of these materials is that they are limited by their stretchability. Developing ultra-compliant, high efficiency organic materials will be of limited utility if the materials are confined only to inert atmospheres.

Graphene has been used in numerous applications as a barrier material in anti-corrosion coatings and molecular gas separation.[16–22] In the field of organic electronics, reduced graphene oxide (rGO) films deposited via spin coating has been used as an encapsulation material in flexible solar cells.[23] However, there is an inverse relationship between barrier properties and transparency for rGO films. rGO films with better barrier properties tend to transmit less light, which can reduce the efficiency of organic optoelectronic devices.[24] Pristine graphene has also been used as an electrode material in flexible solar cells with a "built in" packaging effect.[25] However, the devices themselves were intrinsically limited in their stretchability due to the kapton substrate that the device was built on.

## 1.2 Experimental Design

### 1.2.2 Selection of Materials

Typically, organic solar cells are fabricated using a transparent conducting bottom electrode such as indium tin oxide (ITO) or PEDOT:PSS and an evaporated metal top contact. The device architecture chosen utilizes PEDOT:PSS as both the cathode and anode material. We selected PEDOT:PSS as the transparent conducting electrode, a commonly used electrode material in organic electronics. PEDOT:PSS has been shown to have both high electrical conductivity and crack onset strain when plasticized with a fluorosurfactant.[26] In order to utilize PEDOT:PSS as both the cathode and anode, the work function of one PEDOT:PSS electrode was lowered using poly(ethyleneimine) (PEI).[27]

P3HpT:PCBM was selected as the active layer material since P3ATs are one of the most studied families of conjugated polymers. The mechanical properties of P3ATs have been shown to possess a high dependence on alkyl side chain length. Increasing side chain length results in a more mechanically compliant material with higher ductility and lower elastic modulus.[28] However, increased side chain length also decreases electrical properties such as charge carrier mobility.[29,30] It has been previously shown that P3HpT co-optimizes both electrical and mechanical properties.[31] PEDOT:PSS and P3HpT:PCBM were both chosen due to their favorable mechanical properties in stretchable devices. Although glass is not a stretchable material, it was chosen as the substrate for the devices in order to isolate any additional degradation effects due to the mechanical failure.

Polyurethane (PU) was chosen as the substrate for graphene because of polyurethane's transparency, stretchability, and amenability to thin film transfer processes due to its intrinsically high surface energy. PU films were fabricated using a simple dip coating process that resulted in thicknesses of less than 150 μm. Furthermore, the high surface energy of PU allowed graphene to be easily transferred onto it with no additional processing.

### 1.2.3 Materials

Regioregular poly(3-heptylthiophene) (P3HpT) was purchased from Rieke Materials and used as received. [6,6]-phenyl C61 butyric acid methyl ester (PCBM) was purchased from Sigma-Aldrich. Poly(3,4-ethylenedioxythiophene):poly(styrenesulfonate) (PEDOT:PSS) (Clevios PH1000) was purchased from Heraeus. Dimethylsulfoxide (DMSO) was purchased from BDH. Zonyl fluorosurfactant, chloroform, ortho-dichlorobenzene (ODCB), acetone, and isopropanol were purchased from Alfa Aesar. Polyurethane (PU, Tecoflex SG-80) was donated by Lubrizol and used as received.

### 1.2.4 Fabrication of Graphene/Polyurethane Barrier Films

Graphene on copper was cut into 2.5cm by 2.5cm pieces and taped to a glass slide with kapton tape. Only the edge of the graphene/copper was taped in order to prevent polyurethane from depositing on the underside of the copper during dip-coating. Graphene on copper was dip-coated into a solution of 10% polyurethane dissolved in tetrahydrofuran. The films were allowed to dry for 10 minutes in air to allow the polyurethane to set. The dip-coating process was repeated three times to ensure a film of

appreciable thickness was formed. Resulting films that were too thin would crumple up and stick to themselves after the copper was etched away. The polyurethane/graphene/copper stack was then placed under dynamic vacuum at 90 °C overnight to remove any residual THF in the polyurethane and to remove air bubbles. This process creates polyurethane that is transparent, smooth, and free of bubble defects. A razor was used to cut away the edges of graphene/copper that was covered by kapton tape. The resulting polyurethane/graphene/copper stack was then floated in a solution of 1 molar iron chloride with the copper side of the stack in contact with the iron chloride solution. Films were left in iron chloride for 30 minutes to ensure that all of the copper was etched away. The graphene/polyurethane films were transferred to a deionized water bath using a clean glass slide. After several washing steps, the graphene/polyurethane films were removed from the water with tweezers and allowed to dry.

### 1.2.5 Fabrication of P3HpT:PCBM Solar Cell Devices

A solution of PEDOT:PSS was made from 92.9 wt % Clevios PH 1000 (~0.9−1.2 wt % PEDOT:PSS), 7.0 wt % DMSO, and 0.1 wt % Zonyl. Glass slides (2.5 cm by 2.5 cm) were cleaned by sonication in alconox, deionized water, acetone, and isopropanol for 10 minutes each. This solution was filtered and spin-coated onto a plasma treated glass slide at 500 rpm for 120 seconds followed by 2000 rpm for 30 seconds. A portion of the film was wiped away to allow silver paint to be used to make contact with the top electrode. Films were annealed on a hot plate at 150 °C for 30 min and slow cooled to room temperature. A solution of PEI was made from 1.5 wt % PEI and 98.5 wt % ethanol. This solution was spin-coated on top of the PEDOT:PSS film at 3000 rpm for 30 seconds. The films were annealed at 110 °C for 10 minutes and allowed to slow cool to

room temperature. The photoactive layer of P3HpT:PCBM was then spin-coated on top at 500 rpm for 240 seconds followed by 2000 rpm for 30 seconds. The devices were moved immediately into a nitrogen filled glovebox and annealed at 110 °C for 28 minutes. The top contacts of the devices were fabricated by spin coating PEDOT:PSS on thermal release tape at 500 rpm for 120 seconds. The thermal release tape was then placed on top of the device and annealed at 135 °C for 10 seconds to deactivate the adhesive, transferring the PEDOT:PSS film onto the device. A portion of the P3HpT:PCBM film was removed with chloroform to expose the bottom contact. Silver paint was then deposited on the top and bottom PEDOT:PSS contacts and copper wires were connected to the silver paint to complete the device.

### 1.2.6 Encapsulation of P3HpT:PCBM Solar Cell Devices

A schematic diagram of the architecture used to test the devices can be seen in **figure 1**. A 3D printer was used to fabricate a spacer in order to suspend the graphene/polyurethane film over the solar cell device. The spacer was printed using polylactic acid (PLA) at a temperature of 200 °C. A small aperture (1cm x 1 cm) was left in the center of the spacer to allow for the graphene/PU film to cover.

The graphene/polyurethane films were secured with scotch tape to a computer controlled stage powered by a linear actuator. The films were stretched to varying amounts of strain (0% to 20%) and secured over the aperture on the PLA spacer. A two part five-minute epoxy was mixed according to the manufacturer's instructions and used to seal the edge of the graphene/polyurethane film to the PLA spacer. An excess of epoxy was added to ensure that there were no holes or gaps between the graphene/polyurethane film and the PLA. All devices were encapsulated inside a nitrogen filled glovebox and

allowed to set for a minimum of 5 hours for the epoxy to cure and reach full setting strength.

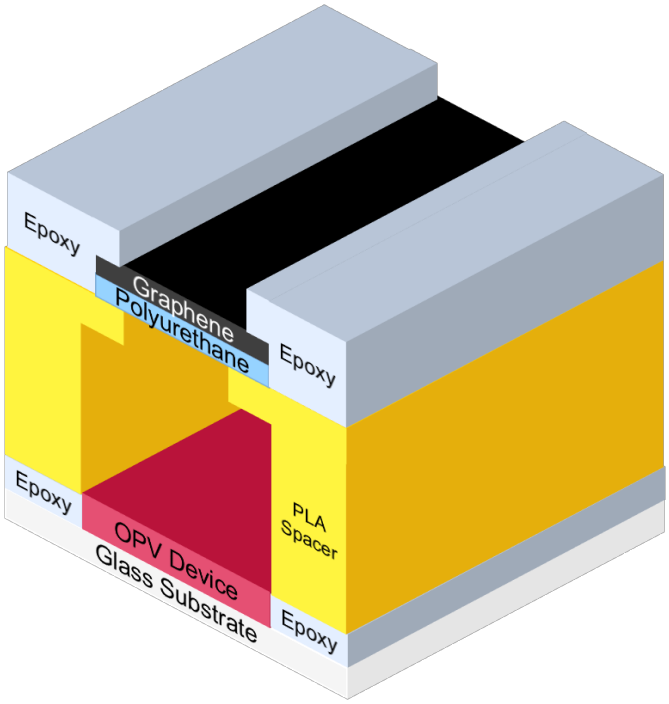


Figure 1) Schematic cross section diagram of architecture used for encapsulation of P3HpT:PCBM devices.

### 1.2.7 Electrical Characterization of Graphene/Polyurethane Films

Graphene/PU films were secured to a linear actuator using scotch tape, as described previously. Eutectic gallium-indium was deposited on opposite ends of the graphene. Electrical contacts were connected using copper wires that were connected to a Keithley 2400 sourcemeter. After each increment of strain, approximately 30s were allowed to elapse in order for the measurement to stabilize.

### 1.2.8 Characterization of Photovoltaic Devices

Devices were removed from the glovebox and tested under illumination from a solar simulator with a 100 mW $cm^{-2}$ flux under AM 1.5G condition. Current densities and voltages were measured using a Keithley 2400 sourcemeter. After being taken out of the glovebox, devices were left in ambient atmosphere.

## 1.3 Results and discussion

### 1.3.2 Characterization of Graphene/Polyurethane Films

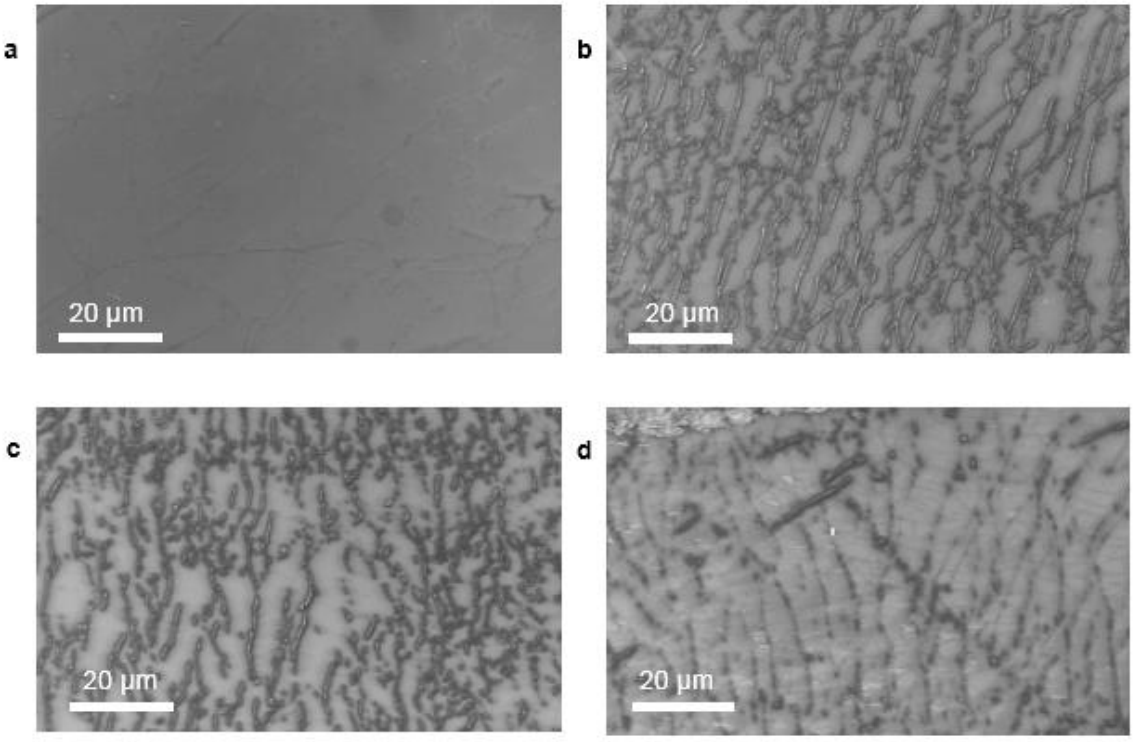


Figure 2) SEM images of graphene on polyurethane strained at a) 0%, b) 3%, c) 5% and d) 20%. "Buckles" are seen in images b and c, while cracks are seen in image d.

The fabricated graphene/polyurethane films were characterized via SEM and electrical resistance measurements. Films at both 0% and 20% strain can be seen in **Figure 2**. At 0% strain, typical defects characteristic of CVD grown graphene can be

observed. The grain boundaries between different graphene crystals appear as faint lines, whereas multilayer defects appear as darker hexagonal regions. At intermediate strains of 3% and 5%, anisotropic features perpendicular to the axis of strain were formed in the film. These features have been reported and determined to be buckles in previous graphene stretching experiments in which graphene was strained, relaxed, and characterized with AFM.[32] At 20% strain, dark anisotropic cracks are formed throughout the film. The features in the film strained at 20% are distinctly different from the features in the films strained at 3% and 5%. The direction of crack formation is perpendicular to the axis of induced strain. The cracks appeared much darker than the rest of the graphene film due to exposure of the non-conducting polyurethane beneath the graphene.

To gain a more quantitative measurement of the crack onset in our films, we measured the electrical resistance of our films as a function of strain. **Figure 3** shows the normalized resistance of a graphene/polyurethane film as a function of strain. At about 6% strain, a major spike in the normalized resistance is observed, suggesting that electrical contact was being broken in the graphene.

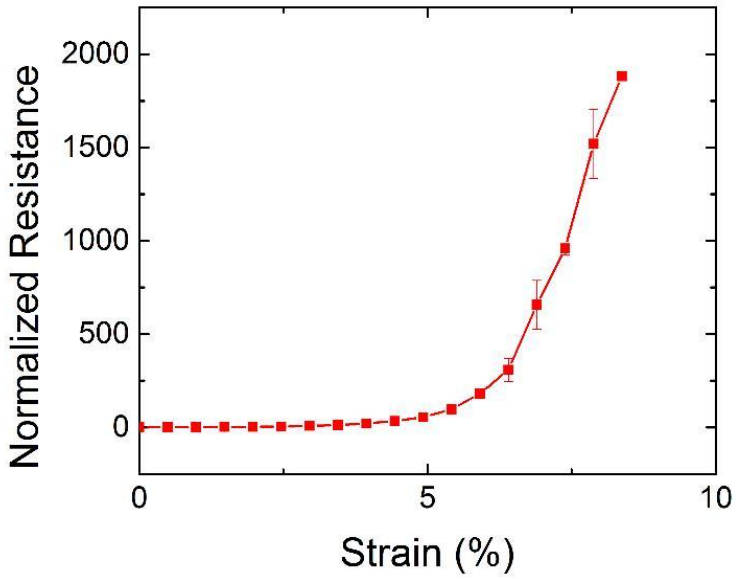


Figure 3) Normalized resistance for graphene on polyurethane that was linearly strained

We also tested the change in normalized resistance as a function of strain cycles for our graphene/polyurethane films. As shown in **Figure 3**, after the first cycle, the normalized resistance does not return to the original resistance value. However, subsequent cycles show that the normalized resistance values remain consistent after the first cycle. When stretched to 3%, the normalized resistance peaks at about 1.2 and slowly lowers as the measurement stabilizes. When returned back to 0% strain, there is a slight hysteresis effect in which the normalized resistance does not go all the way back to 1. The same effect is seen in the film stretched 5%, however, the increase in normalized resistance goes up to ~3 at 5% as opposed to only 1.2 for 3%.

**Figure 4** shows the range of "stable" strains for our graphene/polyurethane films. The plot was produced by straining the barrier film, returning it back to 0% strain, and straining the barrier film slightly more than the previous strain. Below strains of 5%, the normalized resistance stays under 10. However, like the data shown in **Figure 3**, the normalized resistance increases exponentially above strains of 5%.

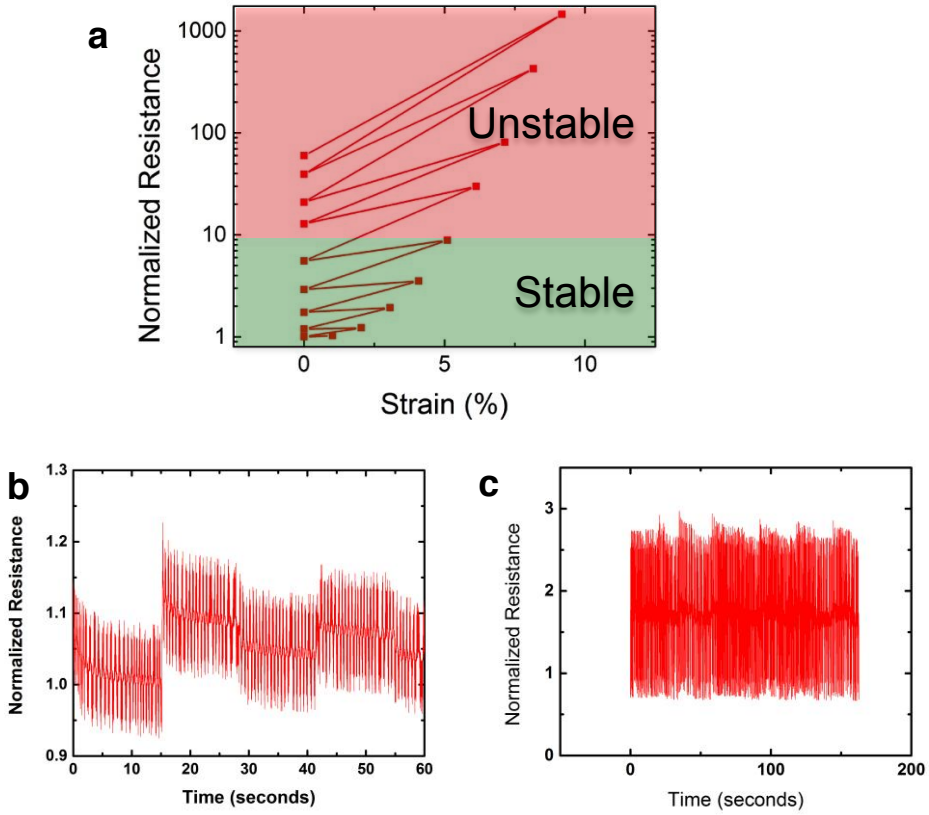


Figure 4) a) Plot of normalized resistance vs. strain for incremental loading of graphene/polyurethane. The film was strained, returned to zero strain, and strained a little more. This process was repeated until electrical conductivity was lost. Bottom: Normalized resistance for graphene on polyurethane under cyclic strains of b) 3% and c) 5%.

### 1.3.3 Effects of Encapsulation

The process of encapsulation did not degrade the photovoltaic properties of the device in any way. **Figure 5** shows the light and dark current vs. density (*JV*) curves both before and after the encapsulation process. The open circuit voltage, short circuit current, and fill factor of the device remained essentially the same after encapsulation. The volatile components of the epoxy used to seal the device did not have any negative effects on the device. This shows that the parameters of the device are not being altered during the process of encapsulation.

### 1.3.4 Solar Cell Degradation Measurements

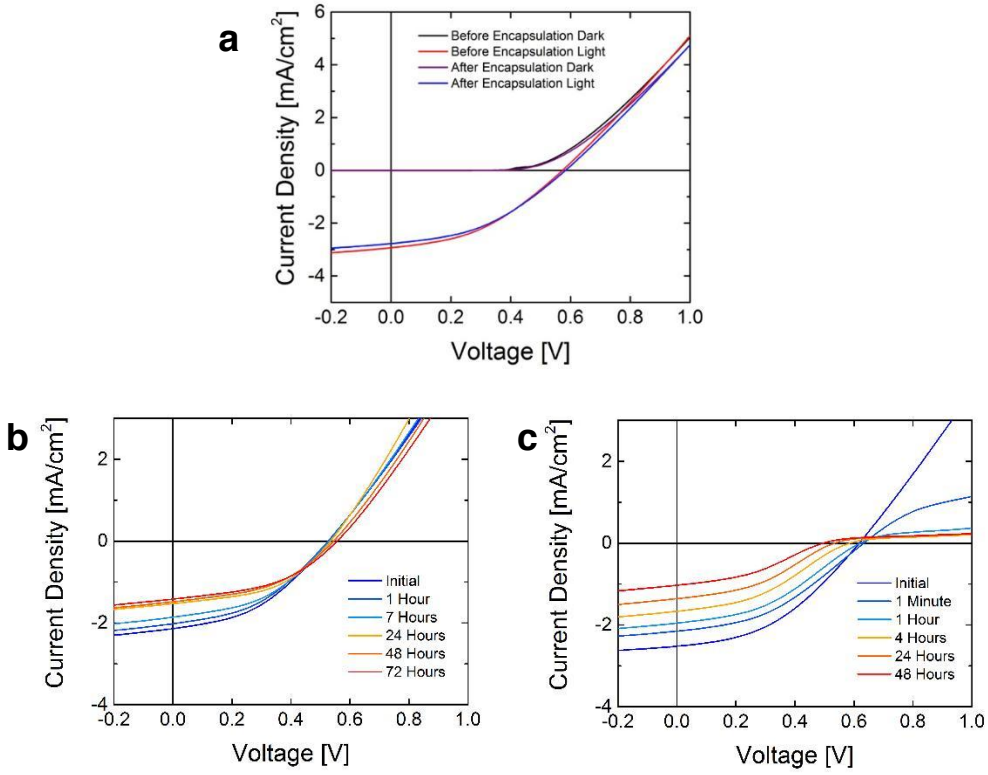


Figure 5) a) Dark and light JV curves before and after encapsulation of device. Bottom: Evolution of JV curves for b) an encapsulated device and c) an unencapsulated device

The evolution of *JV* curves for a device encapsulated with graphene/polyurethane and a device that was unencapsulated is shown in **Figure 5**. The unencapsulated device begins showing signs of degradation as soon as it is exposed to the solar simulator in the presence of ambient atmosphere. The short circuit current of the device begins to drop significantly. Over the course of a several days, the fill factor and open circuit voltage of the unencapsulated device also significantly drops. Once degradation begins, a significant change in the overall shape of the curve occurs. The most noticeable change is the presence of a "tail" region that appears once the open circuit voltage of the device is passed. The change in the overall shape of the curve can be attributed to the chemical degradation occurring the active layer of the device. Once the conjugation in the polymer backbone of the active layer begins to break, charge carrier mobility is greatly reduced. The reduction in mobility results in an increase of series resistance in the device, which is one possible cause for the significant change in the shape of the curve as degradation occurs.

In contrast, the encapsulated device shows a much smaller drop in short circuit current. Furthermore, over the course of several days, the encapsulated device maintains its open circuit voltage and fill factor, showing only a decrease in short circuit current.

Normalized efficiencies were recorded for devices over the course of several days. **Figure 6** summarizes the different barrier types tested. Devices encapsulated with glass and devices with no barrier were also fabricated as controls for this experiment. As expected, the glass encapsulated device performed well compared to the other barriers, retaining about 61.1 ± 3.2% of the original efficiency after ten days. Although glass is considered to be a perfect barrier, the approximately 40% of lost efficiency likely due to

other degradation methods, such as photo-induced degradation of the active layer. Similarly, the unencapsulated device exhibited the greatest degradation, retaining only about 15.1 ± 1.9% of the original efficiency after ten days. A control using polyurethane only (with no graphene) was also fabricated. The PU-only device exhibited an intermediate amount of degradation, retaining 40.0 ± 4.5% of the original efficiency after ten days.

All of the graphene encapsulated devices fell in between the glass control device and the PU-only control device. The unstrained (0%) graphene/PU film performed the best out of the graphene encapsulated devices, retaining 60.6 ± 3.7% of the original efficiency after ten days. This result indicates that the unstrained graphene/PU film in our experiment was comparable to the glass control.

However, the strained graphene/PU films showed slightly worse results compared to that of the unstrained graphene/PU film. The films stretched at 3%, 5%, and 20% retained 39.8± 2.0%, 46.7 ± 5.3%, and 47.7 ± 6.4% of their original efficiencies, respectively. This is comparable to the PU-only film. Although it appears that the 5% and 20% graphene/PU films outperformed the PU-only film, the error bars overlap, indicating that it is not statistically significant enough to be different.

Looking at the initial degradation of the devices after the first day shows more significant results. All of the graphene/PU encapsulated devices show a higher efficiency than the PU-only and no barrier devices. The graphene/PU films are also nearly indistinguishable from each other and from glass after the first day. While the PU-only film drops to 80% efficiency, all of the graphene/PU encapsulated devices fall within the range of about 90%. The difference in apparent barrier properties between one day and

ten days can be attributed to the lag time in the films. The glass and unstrained graphene/PU film have long lag times that greater than the length of this experiment. This is expected, due to glass and unstrained graphene/PU having little to no cracks or defects in the film. Conversely, once graphene/PU films are stretched, cracks are formed allowing oxygen and water vapor to percolate through. Because graphene is intrinsically an excellent barrier material, the time in which it takes gases to diffuse through the cracks is lengthened. However, once gases have completely percolated through the cracks in graphene, the barrier properties of the graphene/PU films will be comparable to that of the PU-only film. As a result, over a longer time period, the strained graphene/PU films begin to act similar to the PU-only film.

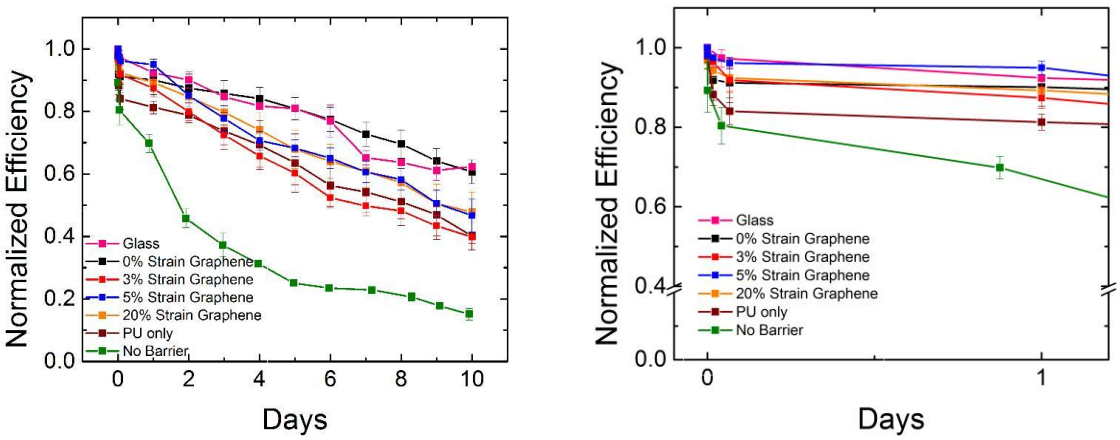


Figure 6) Plot of normalized efficiency vs. time for devices encapsulated with different types of barriers. Left: Degradation measurements over the course of 10 days. Right: Degradation after 1 day.

## 1.4 Conclusions

We demonstrated that graphene/polyurethane barrier films have the potential to be used in stretchable organic electronics. Graphene/polyurethane barrier films that are

unstrained perform as well as glass, while films that are strained maintain good barrier properties over the first day of testing as compared to a device with no barrier at all.

One potential issue with future devices will be the interface between the barrier film and the device itself. Epoxy was used in our work to seal the barrier film and the device, however, epoxy is not stretchable. In order to incorporate these films into an all-polymer device, an alternative method to make the encapsulation seal must be developed.

## 1.5 References


1. Jørgensen, M., Norrman, K. & Krebs, F. C. Stability/degradation of polymer solar cells. *Sol*. *Energy Mater*. *Sol*. *Cells* **92,** 686–714 (2008).

2. Jørgensen, M., Norrman, K., Gevorgyan, S. a., Tromholt, T., Andreasen, B. & Krebs, F. C. Stability of polymer solar cells. *Adv*. *Mater*. **24,** 580–612 (2012).

3. Manceau, M., Rivaton, A., Gardette, J. L., Guillerez, S. & Lemaître, N. The mechanism of photo- and thermooxidation of poly(3-hexylthiophene) (P3HT) reconsidered. *Polym*. *Degrad*. *Stab*. **94,** 898–907 (2009).

4. Hammock, M. L., Chortos, A., Tee, B. C. K., Tok, J. B. H. & Bao, Z. 25th anniversary article: The evolution of electronic skin (E-Skin): A brief history, design considerations, and recent progress. *Adv*. *Mater*. **25,** 5997–6038 (2013).

5. Lipomi, D. J., Tee, B. C.-K., Vosgueritchian, M. & Bao, Z. Stretchable organic solar cells. *Adv*. *Mater*. **23,** 1771–1775 (2011).

6. Shepherd, R. F., Ilievski, F., Choi, W., Morin, S. A., Stokes, A. A., Mazzeo, A. D., Chen, X., Wang, M. & Whitesides, G. M. From the Cover: Multigait soft robot. *Proceedings of the National Academy of Sciences* **108,** 20400–20403 (2011).

7. O 'connor, T. F., Rajan, K. M., Printz, A. D. & Lipomi, D. J. Toward organic electronics with properties inspired by biological tissue. *J*. *Mater*. *Chem*. *B* **3,** 4947–4952 (2015).

8. He, Z., Xiao, B., Liu, F., Wu, H., Yang, Y., Xiao, S., Wang, C., Russell, T. P. & Cao, Y. Single-junction polymer solar cells with high efficiency and photovoltage. *Nat Phot*. **9,** 174–179 (2015).

9. Yang, Y. (Michael), Chen, W., Dou, L., Chang, W.-H., Duan, H.-S., Bob, B., Li, G. & Yang, Y. High-performance multiple-donor bulk heterojunction solar cells. *Nat Phot*. **9,** 190–198 (2015).

10. Leenaerts, O., Partoens, B. & Peeters, F. M. Graphene: A perfect nanoballoon. *Appl*. *Phys*. *Lett*. **93,** (2008).

11. Yoo, B. M., Shin, H. J., Yoon, H. W. & Park, H. B. Graphene and graphene oxide and their uses in barrier polymers. *J*. *Appl*. *Polym*. *Sci*. **131,** 1–23 (2014).

12. Krebs, F. C. Air stable polymer photovoltaics based on a process free from vacuum steps and fullerenes. *Sol*. *Energy Mater*. *Sol*. *Cells* **92,** 715–726 (2008).

13. Jang, W. S., Rawson, I. & Grunlan, J. C. Layer-by-layer assembly of thin film oxygen barrier. *Thin Solid Films* **516,** 4819–4825 (2008).

14. Burrows, P. E., Graff, G. L., Gross, M. E., Martin, P. M., Shi, M. K., Hall, M., Mast, E., Bonham, C., Bennett, W. & Sullivan, M. B. Ultra barrier flexible substrates for flat panel displays. *Displays* **22,** 65–69 (2001).

15. Dennler, G., Lungenschmied, C., Neugebauer, H., Sariciftci, N. S., Latrèche, M., Czeremuszkin, G. & Wertheimer, M. R. A new encapsulation solution for flexible organic solar cells. *Thin Solid Films* **511-512,** 349–353 (2006).

16. Kirkland, N. T., Schiller, T., Medhekar, N. & Birbilis, N. Exploring graphene as a corrosion protection barrier. *Corros*. *Sci*. **56,** 1–4 (2012).

17. Kousalya, A. S., Kumar, A., Paul, R., Zemlyanov, D. & Fisher, T. S. Graphene: An effective oxidation barrier coating for liquid and two-phase cooling systems. *Corros*. *Sci*. **69,** 5–10 (2013).

18. Singh Raman, R. K., Chakraborty Banerjee, P., Lobo, D. E., Gullapalli, H., Sumandasa, M., Kumar, A., Choudhary, L., Tkacz, R., Ajayan, P. M. & Majumder, M. Protecting copper from electrochemical degradation by graphene coating. *Carbon N*. *Y*. **50,** 4040–4045 (2012).

19. Ahlberg, P., Jeong, S. H., Jiao, M., Wu, Z., Jansson, U., Zhang, S. L. & Zhang, Z. Bin. Graphene as a diffusion barrier in galinstan-solid metal contacts. *IEEE Trans*. *Electron Devices* **61,** 2996–3000 (2014).

20. Boutilier, M. S. H., Sun, C., O'Hern, S. C., Au, H., Hadjiconstantinou, N. G. & Karnik, R. Implications of permeation through intrinsic defects in graphene on the design of defect-tolerant membranes for gas separation. *ACS Nano* **8,** 841–849 (2014).

21. Bunch, J. S., Verbridge, S. S., Alden, J. S., Van Der Zande, A. M., Parpia, J. M., Craighead, H. G. & McEuen, P. L. Impermeable atomic membranes from graphene sheets. *Nano Lett*. **8,** 2458–2462 (2008).

22. Nguyen, B. S., Lin, J. F. & Perng, D. C. 1-Nm-Thick Graphene Tri-Layer As the Ultimate Copper Diffusion Barrier. *Appl*. *Phys*. *Lett*. **104,** (2014).

23. Kim, T., Kang, J. H., Yang, S. J., Sung, S. J., Kim, Y. S. & Park, C. R. Facile preparation of reduced graphene oxide-based gas barrier films for organic photovoltaic devices. *Energy Environ*. *Sci*. **7,** 3403–3411 (2014).

24. Becerril, H. A., Mao, J., Liu, Z., Stoltenberg, R. M., Bao, Z. & Chen, Y. Evaluation of solution-processed reduced graphene oxide films as transparent conductors. *ACS Nano* **2,** 463–470 (2008).

25. Liu, Z., Li, J. & Yan, F. Package-free flexible organic solar cells with graphene top electrodes. *Adv*. *Mater*. **25,** 4296–4301 (2013).

26. Lipomi, D. J., Lee, J. A., Vosgueritchian, M., Tee, B. C.-K., Bolander, J. A. & Bao, Z. Electronic Properties of Transparent Conductive Films of PEDOT:PSS on Stretchable Substrates. *Chem*. *Mater*. **24,** 373–382 (2012).

27. Zhou, Y., Fuentes-Hernandez, C., Shim, J., Meyer, J., Giordano, A. J., Li, H., Winget, P., Papadopoulos, T., Cheun, H., Kim, J., Fenoll, M., Dindar, A., Haske, W., Najafabadi, E., Khan, T. M., Sojoudi, H., Barlow, S., Graham, S., Bredas, J.-L., Marder, S. R., Kahn, A. & Kippelen, B. A Universal Method to Produce Low-Work Function Electrodes for Organic Electronics. *Science* **336,** 327–332 (2012).

28. Savagatrup, S., Makaram, A. S., Burke, D. J. & Lipomi, D. J. Mechanical properties of conjugated polymers and polymer-fullerene composites as a function of molecular structure. *Adv*. *Funct*. *Mater*. **24,** 1169–1181 (2014).

29. Savagatrup, S., Printz, A. D., Wu, H., Rajan, K. M., Sawyer, E. J., Zaretski, A. V., Bettinger, C. J. & Lipomi, D. J. Viability of stretchable poly(3-heptylthiophene) (P3HpT) for organic solar cells and field-effect transistors. *Synth*. *Met*. **203,** 208–214 (2015).

30. O'Connor, B., Chan, E. P., Chan, C., Conrad, B. R., Richter, L. J., Kline, R. J., Heeney, M., McCulloch, I., Soles, C. L. & DeLongchamp, D. M. Correlations between mechanical and electrical properties of polythiophenes. *ACS Nano* **4,** 7538–7544 (2010).

31. Savagatrup, S., Printz, A. D., Rodriquez, D. & Lipomi, D. J. Best of both worlds: Conjugated polymers exhibiting good photovoltaic behavior and high tensile elasticity. *Macromolecules* **47,** 1981–1992 (2014).

32. Jiang, T., Huang, R. & Zhu, Y. Interfacial sliding and buckling of monolayer graphene on a stretchable substrate. *Adv*. *Funct*. *Mater*. **24,** 396–402 (2014).